Inorganic Chemistry

ARTICLE

pubs.acs.org/IC

Anticancer Activity, Attenuation on the Absorption of Calcium in Mitochondria, and Catalase Activity for Manganese Complexes of N-Substituted Di(picolyl)amine

Dong-Fang Zhou,[†] Qiu-Yun Chen,*[,†,§] Yan Qi,[†] Hai-Jian Fu,[†,§] Zan Li,[†] Kai-Di Zhao,[‡] and Jing Gao[‡]

[†]School of Chemistry and Chemical Engineering and

[§]School of Pharmacy, Jiangsu University, Zhenjiang, 212013 P .R. China

[‡]State Key Laboratory of Coordination Chemistry, Nanjing University, 210093 P. R. China

Supporting Information

ABSTRACT: In order to find multifunction anticancer complexes, three Mn(II) complexes of N-substituted di(2-pyridylmethyl)amine were characterized and used as agents to interfere with the functions of mitochondria and the metabolite of O_2 in cancer cells. It was found that carboxylate-bridged dimanganese(II) systems are good models of catalase and exhibit good inhibition of the proliferation of U251 and HeLa cells. The inhibiting activity of these manganese(II) complexes on the tumor cells in vitro was related to their disproportionating H_2O_2 activity. The reaction of carboxylate-bridged dimanganese Mn(II) complex with H_2O_2 forms a stable Mn(III)−(μ-O)$_2$−Mn(IV) complex. Extensive experimental results show that chloride-bridged dimanganese(II) complexes could inhibit the swelling of calcium(II) overloaded mitochondria, and carboxylate-bridged manganese(II) complexes enhance the swelling of calcium(II) overloaded mitochondria. These results indicate that the interactions between Mn(II) complexes of N-substituted di(picolyl)amine and mitochondria are influenced by the structure and conformation of the complexes. Mn(II) complexes of N-substituted di(picolyl)amine could be developed as multifunctional anticancer complexes to interfere with the absorption of calcium(II) in mitochondria and the metabolite of O_2 through the H_2O_2 or ROS involved signaling induced apoptosis of cancer cells.

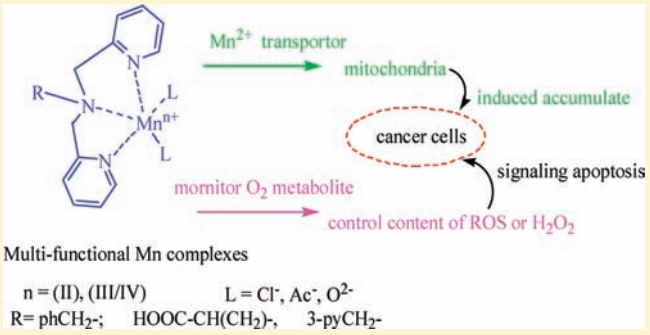

INTRODUCTION

Since the success of cisplatin, more and more attention has been paid to metal complexes, which inhibit the proliferation of cancer cells through a DNA or mitochondria involved path.[1,2] Mitochondria are the most important organelles in determining continued cell survival and cell death. The unique structure and functional characteristics of mitochondria enable the selective targeting of drugs that are designed to modulate the function of these organelles for therapeutic gain.[3] Lonidamine, arsenite, and betulinic acid act directly on mitochondrial membranes and associated proteins to induce membrane permeabilization. Mitochondrial membranes span across a negative potential; most agents have a positively charged moiety that takes advantage of electrostatic forces in locating its target.[4,5] Biochemically active Mn(III)−salen and −salphen complexes induce nuclear fragmentation and the release of cytochrome *c* from the mitochondria to cytosol, indicating the involvement of the mitochondrial pathway of apoptosis.[6] Manganese(II) ions are the required cofactor for many ubiquitous enzymes. Mitochondria can accumulate Mn(II) ions through an ATP-dependent Ca transporter.[7] The transport mechanism of Mn(II) in vivo may make it possible for Mn(II)-based compounds to be tumor-targeted. Research has proven that Mn(II) ions were mainly taken up and transported by a divalent metal transporter (DMT-1) and a transferrin (Tf) receptor (TfR), which were highly expressed in some tumor tissues.[8−10] Simple Mn(II) salts have been reported to exert an antiproliferative effect on several cancer cell lines at rather high concentrations (in the mmol range), but their application was limited because of their high dose.[11] In another study, we found that the Mn(II) complex [(Adpa)Mn(Cl)-(H_2O)] (Adpa = bis(2-pyridylmethyl)amino-2-propionic acid) can also target mitochondria and inhibit the proliferation of human glioma cells (U251) with low IC_{50} (9.5 μM) in vitro.[12] So, it is possible for special Mn(II) complexes to target cancer cells through an ATP-related Ca transporter. Mitochondrial Ca^{2+} loading has profound consequences for mitochondrial function, such as regulating cellular respiration and mediating cell death by apoptosis or necrosis.[8,13] The ability of Ca^{2+} to regulate both cell death and proliferation, combined with the potential for pharmacological modulation, offers the opportunity for a set of new drug targets in cancer.

In addition to the attenuation of the absorption of calcium in mitochondria, most transitional metal complexes of di(picolyl)amine

Received: January 2, 2011
Published: June 28, 2011

were reported as models of nonheme dioxygenase.[14] For example, Mn(II) complexes of bis(2-pyridylmethyl)benzylamine, nonheme mimics, can react with H_2O_2, resulting the intramolecular aromatic hydroxylation (pro-oxidant).[15] The dinuclear manganese complexes with pyridine and (pyridylmethyl)amine ligands were able to catalyze the oxidation of several alkenes to the corresponding epoxides, using H_2O_2 as oxidants.[16] The manganese(II) complex $[Mn_2(\mu\text{-}O_2CCH_3)_3L_2]^+$ (L = bis(pyridylmethyl)amine) and aminopyridine manganese(II) complexes were studied for their ability to disproportionate H_2O_2 and produce highly valued intermediates.[17] These indicated that manganese(II) complexes with the derivatives of bis(2-pyridylmethyl)amine could disproportionate H_2O_2 or react with H_2O_2 to produce an oxidant. Many manganese(II) complexes of N-substituted bis(pyridylmethyl)amine, metalloporphyrin, and Salens were reported as pro-oxidant or as antioxidant.[18] There is no report on whether the manganese(II) complexes could inhibit the proliferation of cancer cells through attenuating the H_2O_2 or O_2 signaling.

Cellular levels of H_2O_2 directly or indirectly play a key role in maglignant transformation and sensitize cancer cells to death. During the overexpression of H_2O_2 detoxifying enzymes or human catalase in vivo, H_2O_2 concentration decreased, and the cancer cells reverted to normal appearance.[19] Cancer cells are more susceptible to H_2O_2 induced cell death than normal cells are. Therefore, it is possible for the manganese(II) complexes of N-substituted di(picolyl)-amines to be multifunctional complexes that inhibit the proliferation of cancer cells through attenuating the absorption of Ca^{2+} and disproportionation of H_2O_2. Here, we report the characterization, interaction with H_2O_2, attenuation of the absorption of Ca^{2+} in mitochondria, and antitumor activities of $[(phdpa)_2Mn_2(\mu\text{-}Cl)_2(Cl)_2]$, $[(pydpa)_2Mn_3(H_2O)_2Cl_6]$, $[(Adpa)_2Mn_2(Ac)(H_2O)_2](Ac)$, and $[(Adpa)Mn(\mu_2\text{-}O)_2Mn(Adpa)]PF_6\cdot 8H_2O$ complexes ((pydpa = *N*-(3-pyridylmethyl)-bis(2-pyridylmethyl)amine; phdpa = *N*-benzyl-bis(2-pyridylmethyl)amine).

EXPERIMENTAL SECTION

Materials and Methods. All chemicals used for synthesis were of reagent grade and used without further purification (Sinopharm Chemical Reagent Co. Ltd., China). Bis(2-pyridylmethyl)amino-2-propionic acid (Adpa), *N*-benzyl-di(pyridylmethyl)amine (phdpa), and $[(phdpa)_2Mn_2(\mu\text{-}Cl)_2(Cl)_2]$ (**1**) were synthesized according to the reported procedures.[12,15] The C, H, and N microanalyses were performed on a Vario EL elemental analyzer. The molar electrical conductivities containing 10^{-4} mol L^{-1} complex were measured at 25.0 ± 0.1 °C using a BSA-A conductometer. The electronic absorption spectra were recorded in the 900−190 nm region using a Varian Cary 50-BIO UV−vis spectrophotometer. The IR spectra were recorded on a Nicolet-470 spectrophotometer in the range 4000−400 cm^{-1}. The ^1H NMR and ^{13}C NMR spectra were measured on a Bruker 400 MHz spectrometer. The electrospray mass spectra (ES-MS) were determined on a Finnigan LCQ mass spectrograph, and the concentration of samples was about 1.0 μmol L^{-1}. The diluted solution was electrosprayed at a flow rate of 5×10^{-6} L^{-1} min^{-1} with a needled voltage of +4.5 kV. The mobile phase was methanol. Electrochemical measurements were carried out on a model 730C Electrochemical Workstation (Shanghai Chenhua Instruments). Analyte concentrations were typically 0.5−1.0 mM in anhydrous acetonitrile containing 0.1 M $[(nBu)_4N]ClO_4$. Unless stated otherwise, a Teflon-shrouded glassy carbon working electrode, a Pt wire auxiliary electrode, and an SCE reference electrode were employed and calibrated externally, using 0.1 mM solutions of ferrocene in 0.1 M $[(nBu)_4N]ClO_4/CH_3CN$). Cyclic voltammograms were obtained at sweep rates between 20 and 100 mV s^{-1}. For reversible processes, the half-wave potential values are reported. Redox potentials are reported ±10 mV.

Synthesis of *N*-(3-Pyridyl)methyl-di(pyridylmethyl)amine (pydpa). A mixture of di(2-picolyl)amine (6 mmol, 1.2 g), pyridylmethyl chloride (6 mmol, 762 mg), and Et_3N (6 mmol, 625 mg) in 25 mL of CH_2Cl_2 was stirred at room temperature for 36 h. Then the solution was washed with 20 mL of 1 M NaOH and water, dried with sodium sulfate, and concentrated to give an oil liquid after column chromatography on silica gel. Yield: 915 mg (60%). Anal. Calcd (%) for $C_{18}H_{18}N_4$: C, 74.46; H, 6.25; N, 19.30. Found: C, 74.52; H, 6.22; N, 19.21. IR (KBr) υ/cm^{-1}: 3010 m, 2924 m, 1674 s, 1588 s, 1474 s, 1430 m, 1356 m, 762 s, 714 s, 622 s. ^1H NMR (400 MHz, $CDCl_3$): δ 3.65 (s, 2H, $-CH_2$(m-Py)), 3.76 (s, 4H, $-CH_2$Py), 7.0−9.0 (m, 12H, Py or m-Py). ^{13}C NMR (400 MHz, $CDCl_3$): δ 55.7 (CH_2−m-Py), 59.9 ($-CH_2$Py), 120−260 (Py or C−m-Py).

Synthesis of $[(pydpa)_2Mn_3(H_2O)_2Cl_6]$ (2). A solution of $MnCl_2\cdot 4H_2O$ (298 mg, 1.5 mmol) in ethanol (10 mL) was added to a stirred ethanol solution (10 mL) of *N*-(3-pyridyl)methyl-di(pyridylmethyl)amine (pydpa) (290.1 mg, 1.0 mmol). The mixture was heated to 70 °C for 1.5 h, and then it was cooled to room temperature. Ethyl ether (20.0 mL) was added to precipitate the products. After filtration, a light yellow solid was obtained. Yield: 384 mg (77%). Anal. Calcd (%) for $C_{36}H_{40}Cl_6Mn_3N_8O_2$: C, 43.49; H, 4.05; N, 11.27. Found: C, 43.56; H, 3.99; N, 11.34. Molar conductance in H_2O (Λ_M): 21 S m^2 M^{-1}. IR (KBr) υ/cm^{-1}: 3317 s, 3058 m, 3012 m, 2925 m, 1648 s, 1601s, 1481 m, 780 s, 673 s, 649 s. UV−vis (H_2O/nm) ($\varepsilon \times 10^{-4}/M^{-1}$ cm^{-1}): 196 (2.36), 260 (1.15).

Synthesis of $[(Adpa)_2Mn_2(Ac)(H_2O)_2](Ac)$ (3). A solution of Adpa (2.0 mmol, 598 mg) in methanol (6 mL) was mixed with $Mn(Ac)_2\cdot 6H_2O$ (2.0 mmol, 508 mg), and then the mixture was refluxed at 80 °C for 1 h. After the solution was cooled, an excess amount of diethyl ether was added, and the obtained yellow brown precipitate was dried under vacuum. Yield: 685 mg (85%). Anal. Calcd (%) for $C_{34}H_{44}Mn_2N_6O_{10}$: C, 50.63; H, 5.50; N, 10.42. Found: C, 50.38; H, 5.38; N, 10.18. Molar conductance in H_2O (Λ_M): 101 S m^2 M^{-1}. IR (KBr) ν/cm^{-1}: 3404 m, 2986, 2911 m, 1604 s, 1572 m, 1475 m, 1442 s, 1380 s, 1312 s, δ(CH, pyridine) 766 s. UV−vis (EtOH/nm) ($\varepsilon \times 10^{-4}/M^{-1}$ cm^{-1}): 215(0.979), 259(1.148). ESI-MS (CH_3OH): m/z = 709.42(100) $[(Adpa)_2Mn_2(\mu\text{-}Ac)]^+$.

Synthesis of $[(Adpa)Mn(\mu_2\text{-}O)_2Mn(Adpa)]PF_6\cdot 8H_2O$ (4). An aqueous solution of H_2O_2 (wt = 30%) (1 mL) was added dropwise to the solution of **3** (1.0 mmol, 808 mg) in water (25 mL) at 0 °C. After the mixture was stirred for 6 h, a dark green solution was obtained. Then KPF_6 (0.54 mmol, 100 mg) was added to the green solution. Green precipitate thus was obtained by filtration, and the dark green crystals suitable for X-ray diffraction studies were obtained by the slow evaporation of the filtrate. Yield: 671 mg (26%). Anal. Calcd (%) for $C_{30}H_{48}F_6Mn_2N_6O_{14}P$: C, 37.09; H, 4.98; N, 8.65.; Found: C, 36.38; H, 4.51; N, 8.68. Molar conductance in DMF (Λ_M): 89 S m^2 M^{-1}. IR (KBr, ν/cm^{-1}): 3427 s, 3083 w, 2987, 2931 w, 1677 s, 1601 s, 1481 m, 1444 s, 1388 m, $\nu(PF_6^-)$ 841 vs, 556 s, δ(CH, pyridine) 781, 763 m, ν(Mn−O−Mn) 698, 680 m, 670 m, 611 m. UV−vis (MeCN/nm) ($\varepsilon \times 10^{-4}/M^{-1}$ cm^{-1}): 210 (2.897), 259 (2.144), 380 (0.137), 440 (0.109), 549 (0.0433), 653 (0.0342). ESI-MS (CH_3OH): m/z = 682.25(22) $[(Adpa)Mn(\mu\text{-}O)_2Mn(Adpa)]^+$, m/z = 209.42(100) $[(Adpa)Mn^{IV}(\mu\text{-}OH)+(Ac)+(H_2O)]^{2+}$ or $[(Adpa)Mn^{III}+(Ac)+2(H_2O)]^{2+}$.

X-ray Crystal Structure Determinations. Crystallographic data for $[(phdpa)_2Mn_2(\mu\text{-}Cl)_2(Cl)_2]$ (**1**), $[(pydpa)_2Mn_3(H_2O)_2Cl_6]$ (**2**), and $[(Adpa)Mn(\mu_2\text{-}O)_2Mn(Adpa)]PF_6\cdot 8H_2O$ (**4**) are listed in Table S1 in the Supporting Information. The crystals of the complexes were selected for lattice parameter determination and collection of intensity data at 293 K on a Rigaku Mercury2 CCD area detector (MSC Inc., 2005) with monochromatized Mo Kα radiation (λ = 0.71073 Å). The data was corrected for Lorenz and polarization effects during the data reduction. A semiempirical absorption correction from equivalents was applied on the basis of multiscans. The structure was solved by direct

methods and refined on F^2 by the full-matrix least-squares methods, using SHELXTL version 5.10.[20] All non-hydrogen atoms were refined anisotropically. Hydrogen atoms were introduced in their calculated positions. All computations were carried out using the SHELXTL-PC program package.

Catalase-like Activity. All of the reactions between the complexes and dihydrogen peroxide were performed in buffered (Tris/Tris-HCl, 0.1 mol L^{-1}, $NaClO_4$ 0.1 mol L^{-1}, pH = 7.1) or water solutions at 0 and 37 °C. The reactivity of the complexes with H_2O_2 was first investigated in water via UV−vis spectroscopy titration at 0 and 37 °C. After the solution (10 mL) of complexes (0.1 mol L^{-1}) was stirred at 0 and 37 °C for 30 min, 0.1 mL of H_2O_2 aqueous solution (30%) was added, and the spectra were recorded at 10 min intervals at 0 °C or 2 min intervals at 37 °C. A similar study was performed using the buffered system (Tris/Tris-HCl, 0.1 mol L^{-1}, $NaClO_4$ 0.1 mol L^{-1}, pH = 7.1).

The volumetric measurements of the evolved dioxygen produced during the reaction of the complexes with H_2O_2 were performed in triplicate as follows: a 10 mL round-bottom flask containing a complex (1.0×10^{-3} mol L^{-1}, 5.0 mL) in MeCN solvent (or a buffered system) was placed in an ice (273.0 ± 0.1 K) bath. The flask was closed with a rubber septum, and a cannula was used to connect the reaction flask to an inverted graduated pipet, filled with water. While the solution containing the complex was being stirred, a solution of 0.5 mL of H_2O_2 aqueous solution was added through the septum using a microsyringe. The volume of oxygen produced was measured in the pipet. The kinetics measurements of complexes **3** and **4** were performed in MeCN solution at 0 °C. Different concentrations of dihydrogen peroxide were prepared by diluting the 30% H_2O_2 aqueous solution with acetonitrile solution or Tris-HCl buffer solution. The optimum reaction order of the substrate with respect to the complexes was determined by reacting different concentrations of complexes with a constant concentration of substrate. Similarly, the optimum reaction order of the complexes with respect to the substrate was determined by reacting different concentrations of substrate with a constant concentration of complexes.

Cytotoxicity Testing. The cytotoxicity assay used two kinds of cell lines (HeLa cells: human cervical cancer cells; and U251 cells: human glioma cells). U251 cells were cultured in RMPI 1640 medium containing 4.8 g/L of HEPES and 2.2 g/L $NaHCO_3$ and supplemented with penicillin/streptomycin (1000 units/mL) and 10% calf serum. HeLa cells were cultured in DMEM medium containing 10% fetal bovine serum. All cells were grown at 37 °C in a humidified atmosphere in the presence of 5% CO_2. Cells were seeded at a density of 4×10^4 cells/mL into 96 sterile well plates and grown in 5% CO_2 at 37 °C. Test complexes were dissolved in H_2O for **1**−**3** (or DMSO for **4**) and diluted with culture media. After 24 h, the complexes were added, and the same samples were kept for 48 h. Cell viability was determined by the 3-[4,5-dimethylthiazol-2-yl]-2,5-diphenpyltetrazolium bromide (MTT) assay by measuring the absorbance at 570 nm with an ELISA reader. IC_{50} was calculated using software provided by Nanjing University. Each test was performed in triplicate. Comparisons were made by one-way analysis of variance. Differences were considered to be significant when $p < 0.05$. All experiments were repeated at least three times.

Mitochondrial Swelling. Liver mitochondria were isolated by conventional differential centrifugation from adult rats.[21] Livers were homogenized in 250 mM sucrose, 1 mM EGTA, and 10 mM HEPES buffer (pH 7.4). The mitochondrial suspension was washed twice in the same medium containing 0.1 mM EGTA, and the final pellet was resuspended in 250 mM sucrose to a final protein concentration of 80−100 mg/mL. Mitochondria (0.4 mg of protein) were incubated in 1.5 mL of a medium containing 125 mM sucrose, 65 mM KCl, 10 mM HEPES-KOH (pH 7.4), and 5 mM potassium succinate (+ 2.5 μM rotenone) at 25 °C. Test complexes were dissolved in H_2O and diluted with culture media. Various concentrations of tested complexes (1−100 μM) were added to the assay mixture. Swelling was initiated by the addition of 50 μM $CaCl_2$ to the sample cuvette at 25 °C. Ciclosporin A (CsA) (5 μM) was used as a positive reference. Mitochondrial swelling was estimated from the decrease in absorbance at 540 nm measured by a Hitachi U-2000 spectrophotometer. The extent of mitochondrial swelling was assayed by measuring the decrease in absorbance (A) at 540 nm, and the inhibitory rate of mitochondrial swelling was calculated as follows: $100(\Delta A_{control} - \Delta A_{drug})/\Delta A_{control}$, $\Delta A = \Delta A_{0\,min} - A$.

Measurement of ROS. ROS levels were measured using the ROS Assay Kit from Beyotime (Beyotime, China), per the manufacturers' protocol.[22]

RESULTS AND DISCUSSION

Characterization of Complexes. The IR spectra show two pyridyl ring bands of υ_{as}(C═N) at approximately 1648 and 1601 cm^{-1} and the δ(CH) vibration of the pyridyl ring at 780 cm^{-1} for complexes **1**−**4**, and all of the bands were shifted compared to the free ligands. These shifts suggest that the nitrogen atom of the pyridyl rings donates a pair of electrons each to the central metal, forming coordinated bands. Two new bands at 680 and 698 cm^{-1} for complex **4** are assigned to the Mn-oxo streching vibration and breath vibrations of high valent Mn(III)−oxo−Mn(IV) (Figure S1 in the Supporting Information). The bis(μ-oxo) $Mn_2^{III,IV}$ bipyridine complex reported by Cooper revealed the Mn−oxo vibration at 676 cm^{-1} and the bis(μ-oxo)$Mn_2^{III,IV}$−bpg (bpg = bis(picolyl)glycylamine) complex at 700 cm^{-1},[16,23] which were similar to the complex **4**, indicating the possible existence of a Mn(III)−oxo−Mn(IV) core. The strong broad peaks at 3317−3400 cm^{-1} for complexes **2**−**4** indicate the existence of water molecules. The bands at 1549 and 1417 cm^{-1} for complexes **3** and **4** were attributed to the antisymmetrical and symmetrical stretching vibrations of the *syn*−*syn* 1,3-bridging acetate.[24] Two strong bands at 814 and 560 cm^{-1} in complex **4** were assigned to the noncoordinated PF_6^-.

A typical absorption band at 259 nm in the UV−vis spectra of complexes **1**−**4** was due to a $\pi \rightarrow \pi^*$ transition involving the pyridine groups of the ligands. Two obvious shoulder bands at 380 nm (ε = 1368) and 440 nm (ε = 1085) and two wider absorption bands at 549 nm (ε = 433) and 653 nm (ε = 342) for complex **4** in MeCN were reminiscent of the ones usually observed for a mixed-valence $Mn^{III}(\mu\text{-O})_2Mn^{IV}$core (Figure 1).[25−28] The bands in the range 400−700 nm belonged to the dimer $Mn^{III,IV}(\mu\text{-O})_2$, for which 430 nm was assigned to an oxo → Mn^{IV} charge-transfer transition (LMCT) and 550 and 630 nm were assigned to the Mn^{IV} d−d transitions, respectively.[25] The band at 430 nm was also assgined to the Mn^{IV} d−d transitions by Krebs.[26] This suggested that complex **4** contained the $[Mn^{III}(\mu\text{-O})_2Mn^{IV}]^{3+}$ core, which was consistent with the crystallography result.

The neutral complex $[(phdpa)_2Mn_2Cl_2(u\text{-}Cl)_2]$ (**1**) could not be detected under the ES-MS conditions, the main peak for **1** at m/z = 380 (100) corresponds to the species $[(phdpa)MnCl]^+$, indicating that the coordinated Cl^- anion could be lost under the ES-MS conditions.[15] The main peak of $[(Adpa)_2Mn_2(Ac)(H_2O)_2](Ac)$ (**3**) at m/z = 709 (100) corresponds to species $[(Adpa)_2Mn_2(\mu\text{-Ac})]^+$, which is formed as a result of the loss of the coordinated two water molecules from $[(Adpa)_2Mn_2(Ac)(H_2O)_2](Ac)$ (**3**) under the ES-MS conditions (Figure S7 in the Supporting Information). The peak for **3** at m/z = 783 (28) corresponds to species $[(Adpa)_2Mn_2(\mu\text{-Ac})(H_2O)+2(CH_3OH)]^+$. The peak of species $[(Adpa)Mn(\mu\text{-O})_2Mn(Adpa)]^+$ at m/z = 682.25 (22) confirms the existence of complex **4** in methanol solution. The main peak at m/z = 209.42 (100) corresponds to the species

dx.doi.org/10.1021/ic200004y |*Inorg. Chem.* 2011, 50, 6929–6937

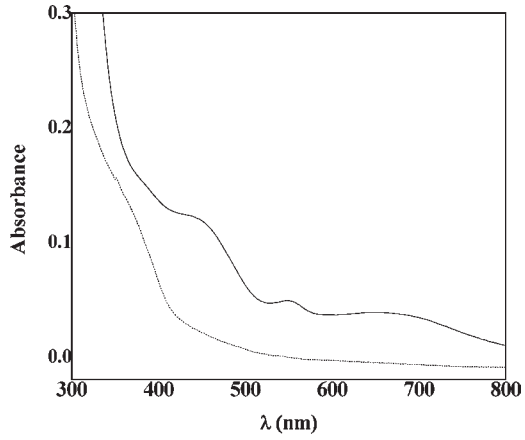

Figure 1. UV spectrum of complexes **3** (···) and **4** (—) in MeCN (C = 0.113 mmol L^{-1}).

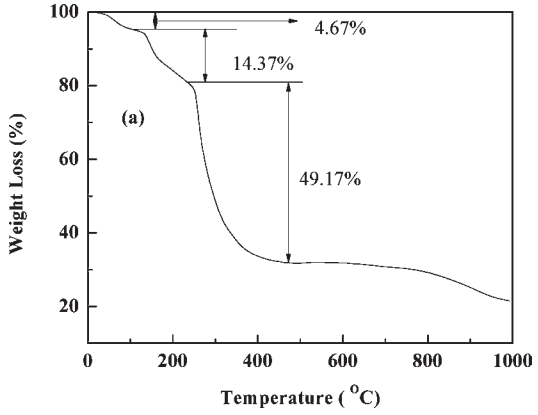

Figure 2. TG plot of complex **3**.

$[(Adpa)Mn^{IV}(\mu\text{-}OH)+(Ac)+(H_2O)]^{2+}$ or $[(Adpa)Mn^{III}+(Ac)+2(H_2O)]^{2+}$. Experimental results indicate that complexes **1** and **4** under the ES-MS conditions could dissociate into mononuclear manganese complexes, but the dinuclear structure of complex **3** is preserved in solution.

DG-TSC. Thermal analysis (TG) curves of **3** in the range 0−1000 °C are shown in Figure 2. The 4.67% weight loss at the range of 25−120 °C corresponds to the loss of two water molecules in **3** (calcd 4.47%). Two Ac^- ions decomposed in the temperature range 120−260 °C, resulting in a 14.37% weight loss (calcd 14.64%). The 49.17% weight loss in the temperature range 260−470 °C corresponds to the loss of two di(pyridylmethyl)-amine groups from the ligand (Adpa) (calcd 49.13%). Thermal analysis results confirm the existence of $[(Adpa)_2Mn_2(Ac)\text{-}(H_2O)_2](Ac)$ (**3**). The 3.90% weight loss in the temperature range 0−160 °C for **2** corresponds to the loss of two coordinated water molecules (calcd 3.83%) (Figure S2a in the Supporting Information). The weight loss of 14.27% at 25−240 °C for **4** is attributed to the loss of eight water molecules (calcd 14.4%) (Figure S2b in the Supporting Information), which is consistent with the crystal structure. In the temperature range 240−500 °C, the 53.1% weight loss corresponds to the further loss of ligands (Adpa) (calcd 55.5%). Thermal analysis results suggest the formation of the titled complexes.

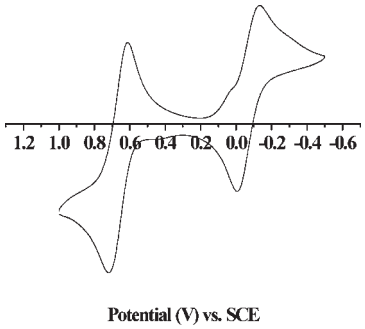

Figure 3. Cyclic voltammogram of complex **4** in MeCN + 0.1 M Bu_4NClO_4. Sweep rate: 100 mV.

Cyclic Voltammogram of Complexes. The cyclic voltammogram (CV) of **4** (1×10^{-3} M) in CH_3CN containing 0.1 M $[(n\text{-}Bu)_4N]ClO_4$ under N_2 is shown in Figure 3. The CV exhibits a single reversible oxidation wave corresponding to the $Mn^{III}Mn^{IV}/Mn^{IV}Mn^{IV}$ redox system ($E_{1/2}$ = 0.71 V; E_{pa} = 0.76 V and E_{pc} = 0.67 V, ΔE_p = 90 mV, scan rate =100 mV s^{-1}) and one poorly reversible reduction wave at $E_{1/2}$ = −0.07 V (E_{pa} = 0.-0.01 V and E_{pc} = −0.13 V, ΔE_p = 120 mV, scan rate = 100 mV s^{-1}) corresponding to the $Mn^{III}Mn^{IV}/Mn^{III}Mn^{III}$. The potentials measured for complex **4** are identical to those described in the literature.[16,18,29]

The cyclic voltammogram (CV) of **1** (1 mM) in CH_3CN containing 0.1 M $[(nBu)_4N]ClO_4$ under N_2 is shown in Figure S3(a) in the Supporting Information. The CV exhibits a reversible oxidation wave corresponding to the $Mn^{II}Mn^{II}/Mn^{III}Mn^{III}$ redox system ($E_{1/2}$ = 0.93 V; ΔE_p = 140 mV, scan rate =100 mV s^{-1}).[30] The cyclic voltammogram (CV) of **3** (1 mM) in CH_3CN containing 0.1 M $[(nBu)_4N]ClO_4$ displays a first irreversible oxidation peak at $E_{1/2}$ = 0.81 V; E_{pa} = 0.61 V and E_{pc}= 1.01 V, ΔE_p = 400 mV, scan rate =100 mV s^{-1}) corresponding to the oxidation of the metallic centers of the complex (Figure S3(b) in the Supporting Information). One poorly reversible oxidation wave at $E_{1/2}$ = 0.39 V (E_{pa} = 0.35 V and E_{pc} = 0.43 V, ΔE_p = 120 mV, scan rate = 100 mV s^{-1}) corresponding to the $Mn^{III}Mn^{III}/Mn^{III}\text{-}Mn^{IV}$, which followed the irreversible oxidation peak at −0.32 V.[18]

Crystal Structure of $[(phdpa)_2Mn_2Cl_2(\mu_2\text{-}Cl)_2]$ (1), $[(pydpa)_2Mn_3(H_2O)_2Cl_6]$ (2), and $[(Adpa)Mn(\mu_2\text{-}O)_2Mn(Adpa)]PF_6\cdot 8H_2O$ (4). The molecular structures of $[(phdpa)_2Mn_2Cl_2(\mu_2\text{-}Cl)_2]$ (**1**) and $[(pydpa)_2Mn_3(H_2O)_2Cl_6]$ (**2**) with the atomic labeling scheme are shown in parts a and b of Figure 4, and the selected bond lengths and angles are listed in parts a and b of Table S2 in the Supporting Information. The Mn2 atom in **1** is coordinated by three N atoms (N1, N2, N3), one chloride atom, and two bridged chloride anions (Cl1, Cl3), resulting in a six coordinate dinuclear Mn(II) complex. The complex $[(phdpa)_2Mn_2Cl_2(\mu_2\text{-}Cl)_2]$ thus shows a distorted octahedral geometry. Atoms N1, N4, Cl1, and Cl3 form the equatorial tetragonal plane (mean deviation = 0.0455), while N2 and Cl4 occupy the apical positions. The Mn1 atom is shifted by 0.3496 Å out of the equatorial plane toward Cl1. The Mn1−N2 and Mn1−Cl4 bond distances are 2.414(4) and 2.4221(17) Å, respectively. The N2−Mn1−Cl4 angle is 159.90(10)°. Atoms N2, N5, Cl1, and Cl3 form the distorted equatorial tetragonal plane (mean deviation = 0.4386), while N6 and Cl2 occupy the apical positions. The Mn2 atom is shifted by 0.3496 Å out of the equatorial plane toward Cl1.

The ligand (pydpa) of **2** acts as a tridentate ligand toward the Mn2 atom. The Mn1 atom in **2** is coordinated by three N atoms

dx.doi.org/10.1021/ic200004y |*Inorg. Chem.* 2011, 50, 6929–6937

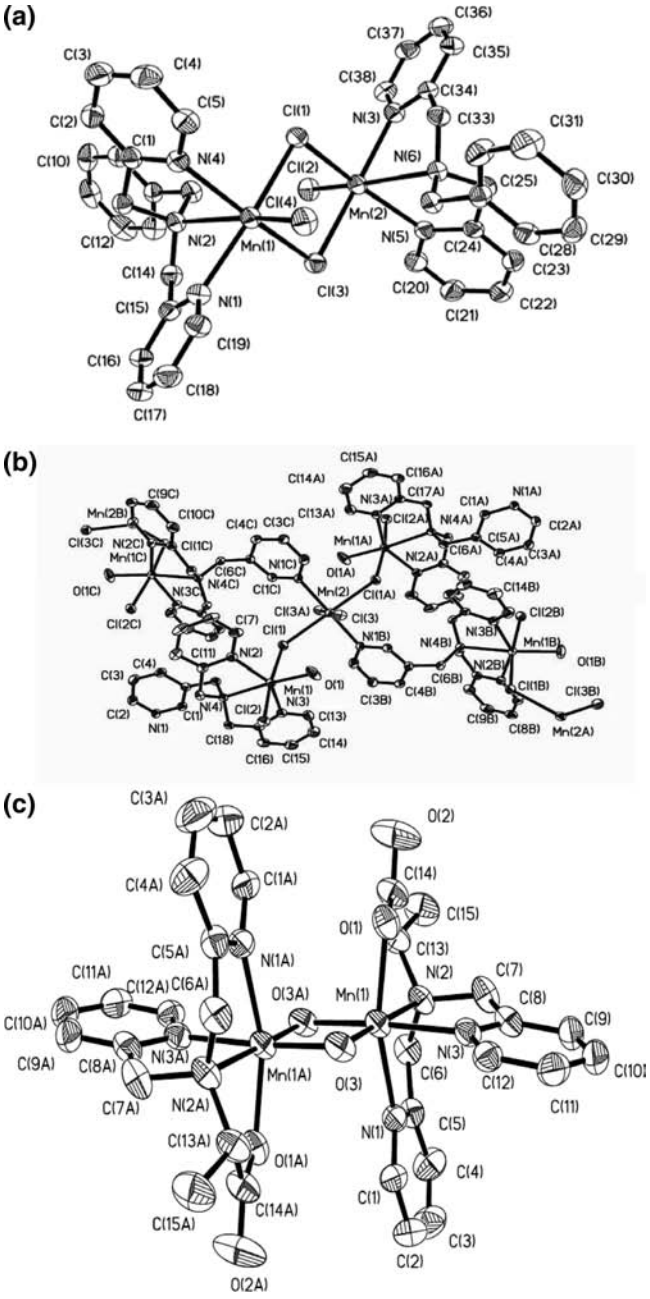

Figure 4. Crystal structures of (a) $[(phdpa)_2Mn_2Cl_2(\mu_2\text{-}Cl)_2]$ (**1**), (b) $[(pydpa)_2Mn_3(H_2O)_2Cl_6]$ (**2**), and (c) $[(Adpa)Mn(\mu_2\text{-}O)_2Mn(Adpa)]^+$ (**4**). Hydrogen atoms are omitted for clarity.

(N2, N3, N4), one oxygen atom (O1) of the water molecule, and two chloride anions (Cl1, Cl2), resulting in a distorted octahedral geometry. Atoms N2, N3, N4, and O1 form the equatorial tetragonal plane (mean deviation = 0.0801), while Cl1 and Cl2 occupy the apical positions. The Mn2 atom is located in the center of the equatorial plane (deviation = 00443 Å). The Cl2−Mn1−Cl1, O1−Mn1−N4, and Cl1−Mn1−N4 angles are 172.79(3), 173.58(9), and 100.06(6)°, respectively. The Cl1 atom of $[(pydpa)_2Mn_3(H_2O)_2Cl_6]$ coordinates with Mn2 as a bridged atom. The Mn2 atom is coordinated by two chloride atoms Cl3, Cl3A $(1.5 + x, 0.5 - y, 0.5 + z)$; two N atoms N1B $(0.5 - x, 1.5 + y, 0.5 + z)$, N1C $(1 - x, -y - 1, 0.5 + z)$; and two bridged chloride atoms Cl1, Cl1A $(1.5 + x, 0.5 - y, z)$ from neighboring molecules, resulting in a octahedral geometry. The Mn2 atom is located in the center of the equatorial plane formed by Cl1A, N1B, N1C, and Cl1 (deviation = 0.0000 Å). The N1B−Mn2−N1C, Cl3A−Mn2−Cl3, and Cl1−Mn2−Cl1A angles are 180°. The structural unit $[(pydpa)Mn(H_2O)(Cl)_2]$ connected through $MnCl_2$ forms a Mn(II) polymer.

Complex **4** crystallizes in the triclinic space group P_{-1} with two complex cations, one hexafluoridophosphate anion, and eight water molecules in the unit cell. The molecular structure of **4** with the atomic labeling scheme is shown in Figure 4c, and selected bond lengths and angles are listed in Table S2c of the Supporting Information. There is a crystallographic inversion center in the middle of the trivalue cation, rendering the two halves of the molecule crystallographically equivalent. Each Mn atom in **4** is coordinated by three N atoms (N1, N2, N3), one oxygen atom (O1) of Adpa, and two oxo bridges (O3, O3A), resulting in a distorted octahedral geometry. Atoms N2, N3, O3, and O3A form the equatorial tetragonal plane (mean deviation = 0.0362), while O1 and N1 occupy the apical positions. The Mn atoms are located in the center of the equatorial plane (deviation = −0.0386 Å). The O1−Mn1−N1 angle is 156.4(11)°. The manganese centers are bridged by two oxo groups, resulting in a metal−metal separation of 2.649(11) Å and a Mn(1)−O(3)−Mn(1A) angle of 93.67(11)°.

The Mn−Mn distance is in the range of intermanganese distances (2.643−2.738 Å) as well as Mn−O−Mn angles (92.36−97.9°) reported for Mn(III,IV) dioxo dimers with tripodal nitrogen donor ligands.[26] The bond lengths for Mn(1)−O(3) and Mn(1)−O(3A), 1.813(3) and 1.819(2) Å, respectively, are shorter than those reported for $[Mn_2(tpa)_2(O)_2]^{2+}$ (tpa = tris(pyridylmethyl)amine) and represent an average for the values of 1.78 Å for Mn(IV) centers and 1.84 Å for Mn(III) centers in valence localized Mn(III, IV) dioxo dimers.[17,26]

Catalase-like Activity of Complexes 1−4 Measured by UV−vis Spectroscopy. The progresses of reactions between complexes and H_2O_2 at various conditions were monitored by UV−vis spectroscopy. When H_2O_2 was added to the white-yellow solution of **3**, the color of the solution became dark-green, but no obvious color change was observed in the reaction solutions containing complexes **1** or **2**. After the addition of 0.1 mL of H_2O_2 (30%) to the aqueous solution of **1** or **2** (1 mM), poorly resolved absorption bands or shoulders between 400 and 700 nm appeared, which indicated that complex **1** or **2** could bind with H_2O_2 and form unstable high value manganese intermediates (Figure S4 in the Supporting Information).

The intensity of four obvious bands or shoulders at 380, 440, 549, and 620 nm for **3** both in buffered solutions and in water solutions increased with the addition of H_2O_2 (Figure 5a). Similar absorption bands were observed when mono- or diunclear Mn(II) complexes containing tripodal ligands HPClNOL or tpa were allowed to react with H_2O_2.[28] These bands were the typical absorptions of the center of $Mn^{III,IV}(\mu\text{-}O)_2$, suggesting that complex **3** could be oxidized by H_2O_2 to form the $[Mn^{III}(\mu\text{-}O)_2Mn^{IV}]^{3+}$ core. The intensity of the typical absorption band at 549 nm for **3** reached its maximum in 2 h (in Tris-buffered solution) and in 3 h (in water) both at 273 K and then decreased gradually (Figure 5a and b). It was also found that the absorption at 549 nm decreased at 310 K in only 8 min, suggesting that the reaction between **3** and H_2O_2 in buffered solutions at 310 K was faster than that carried out in water at 273 K. Experimental results also show that the stability of $[Mn^{III}(\mu\text{-}O)_2Mn^{IV}]^{3+}$ in this system decreased with the increase of temperature.

dx.doi.org/10.1021/ic200004y |*Inorg. Chem.* 2011, 50, 6929–6937

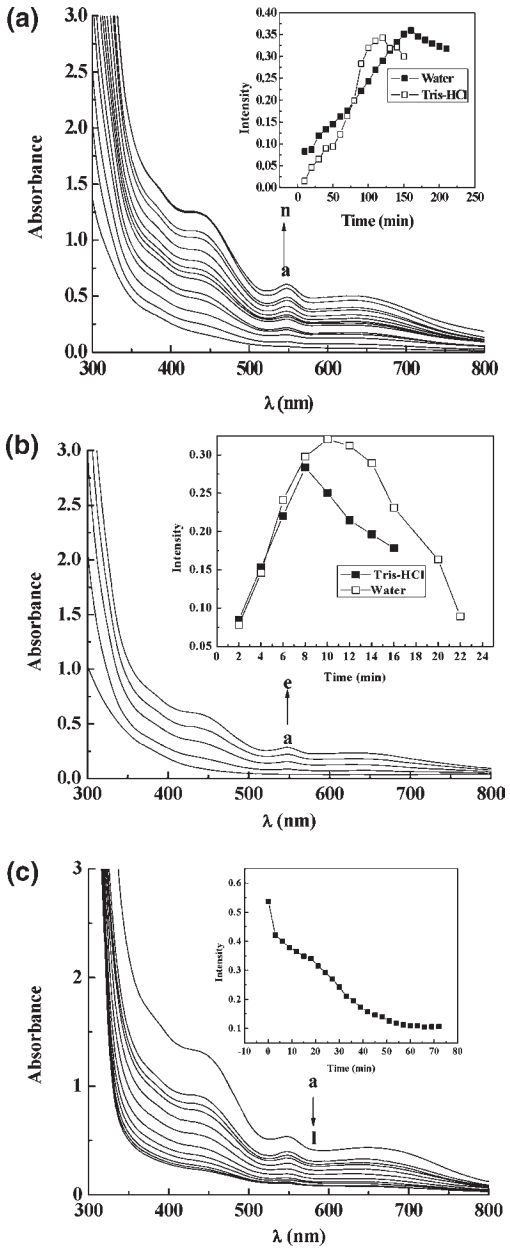

Figure 5. UV−vis spectra for compounds **3** (parts a and b) and **4** (part c) after the addition of H_2O_2 (in MeCN for **4**). Insets show the increase and decrease in intensity of the band at 549 nm. (a) [**3**] = 1 mM, 0.1 mL of 30% H_2O_2 aqueous solution, temperature = 273 K, water as solvent. The spectra were recorded at 10 min intervals (line a, 0 min; line n, 120 min). (b) [**3**] = 1 mM, 0.1 mL of 30% H_2O_2 aqueous solution, temperature = 310 K, Tris-HCl buffer solution. The spectra were recorded at 2 min intervals (line a, 0 min; line e, 8 min). (c) [**4**] = 1 mM, 0.5 mL of 30% H_2O_2 aqueous solution, temperature = 273 K. The spectra were recorded at 3 min intervals (line a, 0 min; line I, 60 min).

The stability of **4** in the presence of H_2O_2 in MeCN was measured by the UV-titration method. The results are shown in Figure 5c. It was found that immediately upon the addition of H_2O_2, there was a sharp decrease in the intensity of the band at 549 nm, which slowed to a gradual decrease, which eventually lead to the disappearance of the band. Then, the color of the solution was changed from dark green to pale yellow. Combined with the UV−vis spectra and the color change of the solution, we deduced that the $[Mn^{III}(\mu\text{-}O)_2Mn^{IV}]^{3+}$ core could be reduced by the H_2O_2 to generate the Mn(II or III) species. The reported Mn(III)/Mn(IV) complex disproportionated H_2O_2 via the III/III and IV/IV oxidation state, in which the III/III oxidation states was an active species.[24−28] The reduced active Mn(II or III) species were further confirmed by the dioxygen evolution of complex **4** (vide infra), which showed a rate increase after 75 min, nearly the same as the equilibrium time of the titration.

Catalase-like Activity Measured by O_2 Evolution—Kinetics Studies. The O_2 volume evolution was used for the study of kinetic of H_2O_2 disproportionation. The H_2O_2 disproportionation promoted by complexes **1**−**3** was carried out in buffered and unbuffered solutions at 0 and 37 °C, and the disproportionation by **4** was carried out in MeCN at 0 °C. It was found that no gas evolution could be monitored when **1** and **2** were incubated with H_2O_2, even after 3 h under the conditions described above, showing that **1** and **2** could not catalyze the disproportionation of dihydrogen peroxide (Figure 5a). This was the same as the reduced oxidation state of Cl^- containing manganese complexes with bipa—Mn(bipa)Cl_2,[26] which also could not disproportionate hydrogen peroxide. The Cl^- inhibition was due to the replacement of a bridging μ-oxygen ligand by bridging μ-Cl^- ligand.[31]

Complexes **3** and **4** can disproportionate dihydrogen peroxide to generate dioxygen. The two complexes can disproportionate 0.2 mL of aqueous H_2O_2 to liberate a similar volume of O_2 (Figure 6a). The kinetic plot is shown in Figure S4 in the Supporting Information. The obtained plot of the initial rate vs the concentration of the dihydrogen peroxide was fitted by using the Hill equation ($V_0 = V_{max}[s]^n/(K_m + [s]^n)$). The parameter K_{cat} was calculated from the equation $K_{cat} = V_{max}/[E_t]$.[32,33] The maximum O_2 evolution rates were about 8.5 and 5.4 mM s^{-1} for **3** in MeCN and in a buffered solution, respectively, and 2.24 mM s^{-1} for **4**. The UV titration of **3** in an aqueous solution by H_2O_2 had demonstrated the formation of **4**. For these conditions, the substrate-dependent catalytic disproportionation of dihydrogen peroxide by complexes **3** and **4** followed similar kinetics (non-Michaelis−Menten kinetics) (Figure S5 in the Supporting Information). The catalytic parameters are shown in Table S3 in the Supporting Information. The similar Hill constants obtained for **3** in both MeCN and buffered solutions are 3.44 ± 0.58 and 3.24 ± 0.37, respectively, and the Hill constant for **4** is 2.07. These show that the catalysts are of a high degree of positive cooperativity.[34] Complexes **3** and **4** exhibit high affinity for dihydrogen peroxide with low K_m values, which are only higher than that of complex $[Mn_2(L^1)(\mu\text{-OAc})(H_2O)]^{2+}$ (L^1 = *N*,*N*,*N*′,*N*′-tetrakis(2-methylenebenzimidazolyl)-1,3-diaminopropan-2-ol).[35] The turnover numbers K_{cat} of the complexes **3** and **4** are 6.28, 9.88, and 3.47, showing that **3** in buffered solution has the highest catalytic activity of disproportionation of dihydrogen peroxide , and the turnover number of **3** is nearly 2- and 3-fold higher than that of **4** in MeCN and in buffered solution, respectively. These turnover numbers were higher than that of $[TPA_2Mn_2(\mu\text{-Cl})_2]^{2+}$ and $[TPA_2Mn_2(\mu\text{-O})_2](ClO_4)_3$[32,33] but were much lower than that of manganese complexes with bpia ligand and *N*,*N*′-bis(3-selenomethylsalicyladehyde-5-sulfonate) bis(1,3)-diamino-2-hydroxypropane) Schiff base.[26]

Complex **3** was considered as a model of the typical carboxylate-bridged dimaganese system, which was key to the activity of dimanganese catalase enzymes.[17,31b] Though the three characterized manganese catalases *Thermus thermophilus* catalase, *Lactobacillus plantarum* catalase, and *Thermoleophilum album* catalase showed much higher catalytic activity of disproportionation of

dx.doi.org/10.1021/ic200004y |*Inorg. Chem.* 2011, 50, 6929–6937

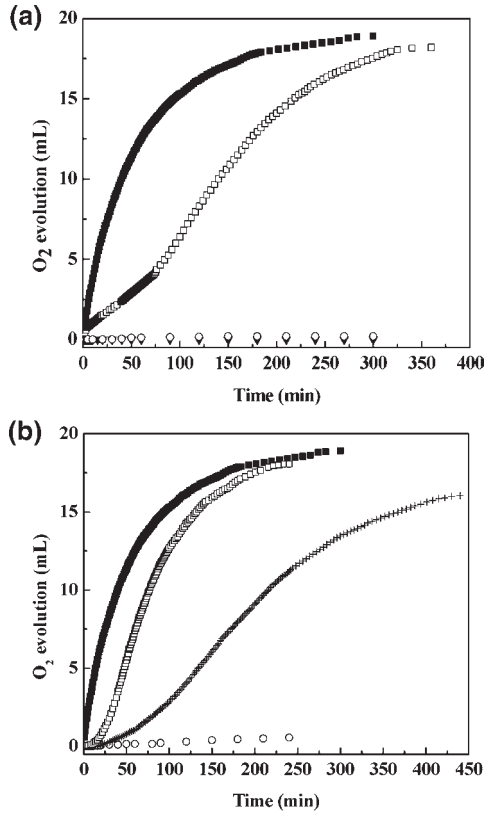

Figure 6. (a) Rates of the O_2 evolution of the complexes at 0 °C in MeCN, [complex] = 1 mM, 0.5 mL of 30% H_2O_2 aqueous solution, V_{MeCN} = 5 mL. **1**(○), **2** (▼), **3** (■), **4** (□). (b) Rates of the O_2 evolution of the complex **3** at different conditions, [**3**] = 1 mM, 0.5 mL of 30% H_2O_2 aqueous solution, $V_{solvent}$ = 5 mL. 0 °C in MeCN (■), 37 °C in Tris-HCl (□), 0 °C in Tris-HCl (+), 37 °C in Tris-HCl without **3** (○).

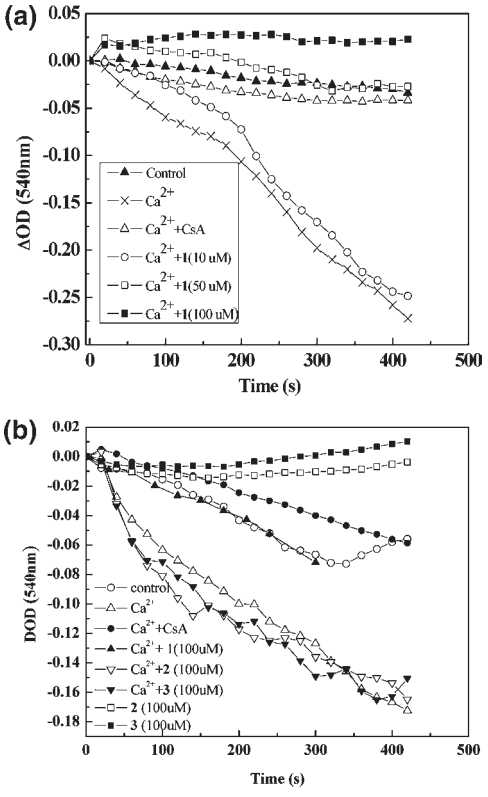

Figure 7. (a) Inhibition of the swelling of Ca^{2+} loaded mitochondria for **1**. Data are mean values for three experiments. Standard deviation <0.06. (b) Inhibition of the swelling of Ca^{2+} loaded mitochondria for **1**, **2**, and **3** in 100 μM. Standard deviation <0.06.

dihydrogen peroxide than **3** and **4**, the activities of the synthetic catalase mimics **3** and **4** were remarkable (Table S3).[36−38] Although **4** was in the oxidation state considered to be the catalytically inactive, "superoxidized" form of manganese catalase, as mentioned earlier,[26] it could catalyze the disproportionation of H_2O_2 in MeCN. According the results, the intrinsic H_2O_2 disproportionation activities of the complexes were in the order **3** > **4** > **1** = **2**.

The catalase activity of **3** under different conditions is shown in Figure 6b. Though a similar maximum volume of dioxygen was liberated under different conditions, the maximum dioxygen evolution rates were 5.4 mM s^{-1} in MeCN and 8.5 mM s^{-1} in the Tris-HCl solution at 37 °C. Experimental results show that there was a lag phase when the reaction was performed in Tris-HCl solution at 0 °C, resulting from the formation of the active species after the addition of H_2O_2, which was much longer than in the reaction that was performed at 37 °C (3 min). When the reaction was carried out in the Tris-HCl solution at 37 °C, the dioxygen evolution rate was 2-fold that of the reaction carried out at 0 °C. The time needed to disproportionate 0.2 mL of H_2O_2 was 4 h at 37 °C, but it was more than 7 h at 0 °C. These results indicated that complex **3** showed higher catalase activity in Tris-HCl solution, and higher temperature accelerated this reaction. The condition of the reaction carried out at 37 °C in Tris-HCl solution was the mimetic condition of the cell environment. Thus, we deduced that complex **3** would also show good catalase activity in vitro.

Interaction with Mitochondria. Mitochondrial swelling is an important method to detect mitochondrial functions.[22,39] The interaction of the Mn(II) complexes with mitochondria was studied by measuring the Ca^{2+} loaded mitochondrial swelling. The Ca^{2+} loaded mitochondria swelling was enhanced in the presence of complexes **2**, **3**, and **4** (100 μM) (Figure 7 and Figure S6 parts a and b in the Supporting Information), which is different from the case of previously reported Mn(II) complex $[(Adpa)Mn(Cl)(H_2O)]$[12] and similar to the case of previously reported nanoparticles dpa-$MnCl_2$@SiO_2.[12,40] However, **1** can inhibit the swelling of Ca^{2+} loaded mitochondria, which indicates that an interaction between the Mn(II) complex and mitochondria exists.[12,39] Mitochondria are involved in the maintenance of intracellular Ca^{2+} homeostasis. One feature of tumor cells is their dependence on glycolysis for ATP generation, which induces the release of Ca^{2+} from the endoplasmic reticulum and leads to enhanced uptake of Ca^{2+} by mitochondria. The complex **1** can inhibit the swelling of Ca^{2+} overloaded mitochondria, indicating that this complex may interfere with the Ca^{2+} transport system just as manganese (Mn^{2+}) does. The Mn(II) complexes **2** and **3** slightly increased the Ca^{2+} loaded mitochondrial swelling, indicating that complexes **2** and **3** interact with mitochondria differently than Mn(II) ions do because the swelling of Ca^{2+} loaded mitochondria was inhibited completely in the presence of 100 μM $MnCl_2$.[12] Experimental results indicate that the interaction between manganese(II) complexes of N-substituted di(picolyl) amine and mitochondria is influenced by their structure and conformation. The mechanism for how the Mn(II) complexes influence the Ca^{2+} uptake needs further investigation.

dx.doi.org/10.1021/ic200004y |*Inorg. Chem.* 2011, 50, 6929–6937

Table 1. IC_{50} Values of Complexes of Three Cancer Cell Lines[a] (μmol/L ± S.D.)

complex	U251	Hela
1	60 ± 0.6	64 ± 0.6
2	51.7 ± 0.6	69.4 ± 0.6
3	35.8 ± 0.4	23.1 ± 0.4
4	6.2 ± 0.4	15.2 ± 0.4
5-Fu	32 ± 0.4	32 ± 0.4
KPF_6	>100	>100
$MnCl_2$	>100	>100

[a] All IC_{50} values were expressed as mean values of the three experiments.

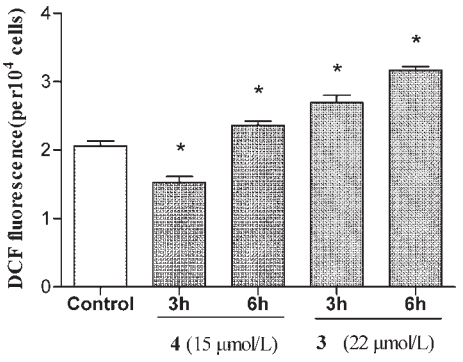

Figure 8. Effect on the ROS content in HeLa for **3** and **4**.

Inhibition of the Proliferation of Cancer Cells. Complexes **1**−**4** were studied for their antitumor activity in vitro by determining the inhibitory percentage against growth of cancer cells U251 and HeLa using the method of 3-[4,5-dimethylthiazol-2-yl]-2,5-diphenpyltetrazolium bromide reduction (MTT method). The IC_{50} values are shown in Table 1. It is interesting to find that **1** and **2** show low anticancer activities with IC_{50} larger than 50 μM. Complexes **3** and **4** were active against the two cancer cell types. Complex **4** can inhibit the proliferation of the U251 cancer cell with IC_{50} = 6.2 μM, which is more active than Mn(III)-salphen and Mn(III)-salnaphen, whose IC_{50} values are 17.83 and 25 for CCL228 cells.[27] The inhibiting activities of the divalent manganese(II) complex **3** on the cancer cells are better than those of **1** and **2**, which correlated with their H_2O_2 disproportionating activities.

Cancer cells are more susceptible to H_2O_2 induced cell death than normal cells. In tumor cells, H_2O_2 concentration is controlled by catalase.[41] So H_2O_2 is considered a mediator of apoptotic cell death. The effect of **3** and **4** on the level of ROS is shown in Figure 8. Extensive experimental results show that complex **3**, a good model of catalse, could induce the increase of ROS level in HeLa cells, indicating that **3** may initiate ROS-mediated death of cancer cells. High value manganese(III/IV) complex **4** causes the decrease of ROS in 3 h, possibly as a result of the good bind of ROS with **4**, which is in agreement with the result of the UV−vis titration. The increase of ROS level in 6 h for **4** may be the result of the death of cancer cells signaling the production of ROS. So we deduced that complexes **3** and **4** may induce cancer cell death in different paths. Cancer cells use O_2 to generate excessive levels of the reactive oxygen species (ROS) and H_2O_2. This alteration in the metabolism of O_2 (dysoxic metabolism) is a common feature of cancer cells and plays an important role in carcinogenesis.[37] Since H_2O_2 is considered a mediator of apoptotic cell death, the elimination of the H_2O_2 and alteration in the metabolism of O_2 is an important path to find multifunctional anticancer compounds. The low IC_{50} for complex **3** is possible as a result of its attenuation of the metabolism of O_2 combined with the antioxidant (mimics of catalase) and prooxidant.

CONCLUSION

The catalase activities of manganese(II) complexes of N-substituted di(2-pyridylmethyl)amine were influenced by their structures and conformations. The carboxylate-bridged dimaganese system is a good model of catalase, with properties of inhibition of the proliferation of U251 and HeLa. The high inhibiting activity of **3** on the tumor cells in vitro may be due to its good disproportionating H_2O_2 activity. Reaction of carboxylate-bridged dimaganese Mn(II) complex **3** with H_2O_2 forms a stable Mn(III)-(μ-O)$_2$-Mn(IV) complex **4**, which also can inhibit the proliferation of cancer cells. So, we deduced that **3** could be used as a prodrug of **4**. In addition, manganese(II) complexes of N-substituted di(2-pyridylmethyl)amine show different effects on the absorption of calcium(II) in mitochondria. It is interesting to find that only **1** exhibits good inhibition of the swelling of calcium(II) overloaded mitochondria, and complexes **2**−**4** could enhance the swelling of calcium(II) overloaded mitochondria. These indicate that the interaction between Mn(II) complexes of N-substituted di(picolyl) amine and mitochondria is influenced by their structure and conformation. Cancer cells use O_2 to generate excessive levels of the reactive oxygen species (ROS) and H_2O_2. The alteration in the metabolism of O_2 by Mn(II) complexes plays an important role in carcinogenesis. Mn(II) complexes of N-substituted di(picolyl) amine could be developed as multifunctional anticancer complexes through attenuating the absorption of calcium(II) in mitochondria and interfering the metabolite of O_2 formed by H_2O_2 or ROS involved signaling induced apoptosis of cancer cells.

ASSOCIATED CONTENT

Supporting Information. IR spectrum (Figure S1), TG-DSC (Figure S2), UV−vis spectra of **2** (Figure S3), CV of **1** and **3** (Figure S4), kinetic plot of complexes (Figure S5), ES-MS spectrum (Figure S7), crystal structures of complexes (Table S1−S2), catalytic activity of manganese catalases and synthetic catalase mimics (Table S3), and swelling of mitochondria (Figure S6). This material is available free of charge via the Internet at http://pubs.acs.org.

AUTHOR INFORMATION

Corresponding Author

*Telephone: +86 0511 8879800. Fax: +86 0511 88791602. E-mail address: chenqy@ujs.edu.cn.

ACKNOWLEDGMENT

Financial support for this study came from the National Science Foundation of China (20971059), the distinguished scholar science foundation of Jiangsu University (06JDG050), and theCoordination Chemistry State Key Laboratory Foundation of Nanjing University.

REFERENCES

(1) Ronconi, L.; Sadler, P. J. *Coord. Chem. Rev.* **2007**, *251*, 1633–1648.
(2) Fulda, S.; Galluzzi, L.; Kroemer, G. *Nat. Rev. Drug Discovery* **2010**, *9*, 447–464.
(3) Galluzzi, L.; Morselli, E.; Kepp, O.; Vitale, I.; Rigoni, A.; Vacchelli, E.; Michaud, M.; Zischka, H.; Castedo, M.; Kroemer, G. *Mol. Aspects Med.* **2010**, *31*, 1–20.
(4) Hoye, A. T.; Davoren, J. E.; Wipf, P.; Fink, M. P.; Kagan, V. E. *Acc. Chem. Res.* **2008**, *41*, 87–97.
(5) Muscella, A.; Calabriso, N.; Fanizzi, E. P.; Pascali, S. A. D.; Urso, L.; Ciccarese, A.; Migoni, D.; Marsigliante, S. *Br. J. Pharmacol.* **2008**, *153*, 34–41.
(6) Ansari, K. I.; Kasiri, S.; Grant, J. D.; Mandal, S. S. *Dalton Trans.* **2009**, 8525–8531.
(7) Camara, K. S.; Lesnefsky, E. J.; Stowe, D. F. *Antioxid. Redox. Signaling* **2010**, *13*, 279–347.
(8) Frezza, C.; Gottlieb, E. *Semin. Cancer Biol.* **2009**, *19*, 4–15.
(9) Aschner, M.; Ruilarte, T. R.; Schneider, J. S.; Zhang, W. *Toxicol. Appl. Pharmacol.* **2007**, *221*, 131–147.
(10) Calzolari, A.; Oliviero, I.; Deaglio, S.; Mariani, G.; Biffoni, M.; Sposi, N. M.; Malavasi, F.; Peschle, C.; Testa, U. *Blood Cells, Mol., Dis.* **2007**, *39*, 82–91.
(11) Sciot, R. P.; Eyken, V.; Desmet, V. J. *Histopathology* **1990**, *16*, 59–62.
(12) Chen, Q. Y.; Zhou, D. F.; Huang, J.; Guo, W. J.; Gao, J. *J. Inorg. Biochem.* **2010**, *104*, 1141–1149.
(13) Monteith, G. R.; Andrew, D. M.; Faddy, H. M.; Robert-Thomson, S. J. *Nat. Rev. Cancer* **2007**, *7*, 519–529.
(14) Wurtele, C.; Sander, O.; Lutz, V.; Waitz, T.; Tuczek, F.; Schindler, S. *J. Am. Chem. Soc.* **2009**, *131*, 7544–7545.
(15) Li, J. F.; Chen, Q. Y. *Spectrochim. Acta, Part A* **2009**, *73*, 25–28.
(16) Dubois, L.; Pecaut, J.; Charlot, M. F.; Baffert, C.; Collomb, M. N.; Deronzier, A.; Latour, J. M. *Chem.—Eur. J.* **2008**, *14*, 3013–3025.
(17) (a) Romero, I.; Dubois, L.; Collomb, M. N.; Deronzier, A.; Latour, J. M.; Pecaut, J. *Inorg. Chem.* **2002**, *41*, 1795–1806. (b) Groni, S.; Dorlet, P.; Blain, G.; Bourcler, S.; Guillot, R.; Anxolabehere-Mallart, E. *Inorg. Chem.* **2008**, *47*, 3166–3172.
(18) (a) Collomb, M. N.; Mantel, C.; Romain, S.; Duboc, C.; Lepretre, J. C.Pecaut, J.; Deronzier, A. *Eur. J. Inorg. Chem.* **2007**, 3179–3187. (b) Davies, C. J.; Fawcett, J.; Shutt, R.; Solan, G. A. *Dalton Trans.* **2005**, 2630–2640. (c) Day, J. D. *Biochem. Pharmacol.* **2009**, *77*, 285–296.
(19) López-Lázaro, M. *Cancer Lett.* **2007**, *252*, 1–8.
(20) Sheldrick, G. M. *SHELXL-97 Program for the Refinement of Crystal Structures*; University of Göttingen: Göttingen, Germany, 1997.
(21) Lee, C. S.; Han, J. H.; Jang, Y. Y.; Song, J. H.; Han, E. S. *Neurochem. Int.* **2002**, *40*, 361–369.
(22) Liu, H. L.; Xu, J. J.; Dai, X. M.; Shi, J. B.; Xu, S.; Gao, J.; Yao, Q. Z.; Liu, F. *J. Appl. Toxicol.* **2009**, *29*, 489–495.
(23) Cooper, S. R.; Calvin, M. *J. Am. Chem. Soc.* **1977**, *99*, 6623–6630.
(24) Biava, H.; Palopoli, C.; Duhayon, C.; Tuchagues, J.-P.; Signorella, S. *Inorg. Chem.* **2009**, *48*, 3205–3214.
(25) Gamelin, D.; Kirk, M.; Stemmler, T.; Pal, S.; Armstrong, W.; Penner-Hahn, J.; Solomon, E. *J. Am. Chem. Soc.* **1994**, *116*, 2392–2399.
(26) (a) Triller, M. U.; Hsieh, W. Y.; Pecoraro, V. L.; Rompel, A.; Krebs, B. *Inorg. Chem.* **2002**, *41*, 5544–5554. (b) Day, J. D. *Biochem. Pharmacol.* **2009**, *77*, 285–296.
(27) Ansari, K. I.; Grant, J. D.; Kasiri, S.; Woldemariam, G.; Shrestha, B.; Mandal, S. S. *J. Inorg. Biochem.* **2009**, *103*, 818–826.
(28) Lessa, J. A.; Horn, A.; Bull, E. S.; Rocha, M. R.; Benassi, M.; Catharino, R. R.; Eberlin, M. N.; Casellato, A.; Noble, C. J.; Hanson, G. R.; Schenk, G.; Silva, G. C.; Antunes, O. A. C.; Fernandes, C. *Inorg. Chem.* **2009**, *48*, 4569–4579.
(29) (a) Suzuki, M.; Senda, H.; Kobayashi, Y.; Oshio, H.; Uehara, A. *Chem. Lett.* **1988**, 1763–1764. (b) Nishida, Y.; Akamatsu, T.; Tsuchiya, K.; Skamoto, M. *Polyhedron* **1994**, *13*, 2251–2254.
(30) (a) Boer, J. W. D.; Browne, W. R.; Brinksma, J.; Alsters, P. L.; Hage, R.; Feringa, B. L. *Inorg. Chem.* **2007**, *46*, 6353–6372. (b) Romero, I.; Collomb, M. N.; Deronzier, A.; Llobet, A.; Perret, E.; Pécaut, J.; Pape, L. L.; Latour, J. M. *Eur. J. Inorg. Chem.* **2001**, 69–72.
(31) (a) Waldo, G. S.; Penner-Hahn, J. E. *Biochemistry* **1995**, *34*, 1507–1512. (b) Boer, J. W.; Browne, W. R.; Feringa, B. L.; Hage, R. *C. R. Chim.* **2007**, *10*, 341–354. (c) Barynin, V. V.; Hempstead, P. D.; Vagin, A. A.; Antonyuk, S. V.; Melik-Adamyan, W. R.; Lamzin, V. S.; Harrison, P. M.; Artymiak, P. J. *J. Inorg. Biochem.* **1997**, *67*, 196–198.
(32) Shin, B. K.; Kim, M. Y.; Han, J. H. *Polyhedron* **2010**, *29*, 2560–2568.
(33) Shin, B. K.; Kim, M. Y.; Han, J. H. *Polyhedron* **2007**, *26*, 4557–4566.
(34) Weiss, J. N. *FASEB J.* **1997**, *11*, 835–841.
(35) (a) Boelrijk, A. E. M.; Dismukes, G. C. *Inorg. Chem.* **2000**, *39*, 3020–3028. (b) Mathur, P.; Crowder, M.; Dismukes, G. C. *J. Am. Chem. Soc.* **1987**, *109*, 5227–5233. (c) Pessiki, P. J.; Khangulov, S. V.; Ho, D. M.; Dismukes, G. C. *J. Am. Chem. Soc.* **1994**, *116*, 891–897. (d) Pessiki, P. J.; Dismukes, G. C. *J. Am. Chem. Soc.* **1994**, *116*, 898–903.
(36) Shank, M; Barynim, V.; Dismukes, G. C. *Biochemistry* **1994**, *33*, 15433–15436.
(37) (a) Kono, Y.; Fridovich, I. *J. Biol. Chem.* **1983**, *258*, 6015–6019. (b) Beyer, W. F., Jr.; Fridovich, I. *Biochemistry* **1985**, *24*, 6460–6467.
(38) Allgood, G. S.; Perry, J. J. *J. Bacteriol.* **1986**, *168*, 563–567.
(39) Mohammadi-Bardbori, A.; Ghazi-Khansari, M. *Toxicol. Mech. Methods* **2007**, *17*, 87–91.
(40) Chen, Q. Y.; Wang, L. Y.; Zhang, L. R.; Guo, W. J.; Gao, J. *Sci. China, Ser. B: Chem.* **2010**, *53*, 1728–1732.
(41) López-Lázaro, M. *Mol. Med.* **2010**, *16* (3−4), 144–153.